

Face Liveness Detection with Component Dependent Descriptor

Jianwei Yang

Zhen Lei

Shengcai Liao

Stan Z. Li*

Center for Biometrics and Security Research & National Laboratory of Pattern Recognition
Institute of Automation, Chinese Academy of Sciences, China

{jwyang, zlei, scliao, szli}@cbsr.ia.ac.cn

Abstract

Spoofing attacks mainly include printing artifacts, electronic screens and ultra-realistic face masks or models. In this paper, we propose a component-based face coding approach for liveness detection. The proposed method consists of four steps: (1) locating the components of face; (2) coding the low-level features respectively for all the components; (3) deriving the high-level face representation by pooling the codes with weights derived from Fisher criterion; (4) concatenating the histograms from all components into a classifier for identification. The proposed framework makes good use of micro differences between genuine faces and fake faces. Meanwhile, the inherent appearance differences among different components are retained. Extensive experiments on three published standard databases demonstrate that the method can achieve the best liveness detection performance in three databases.

1. Introduction

Generally, the sources of illegal attacks mainly consist of printing photograph, screen images or videos, ultra-realistic face masks or a 3-D model of an authorized client. Among these types of attacks, the most flexible one is printing photographs or screen images captured from internet. Secure FR systems demand much for the capability of liveness detection (also known as anti-spoofing), which can identify whether a face is from a real client or only the portrait.

Existing face anti-spoofing approaches can be mainly categorized into three groups: interaction-based approaches, multi-spectral illumination based and micro-textures based ones. Interaction-based approaches aims at detecting the physiological response of face. This response can be represented by biometric motions, such as eye blinking [23, 18], head rotation [2], mouth movement [13], and the holistic motion [12]. These approaches are vulnera-

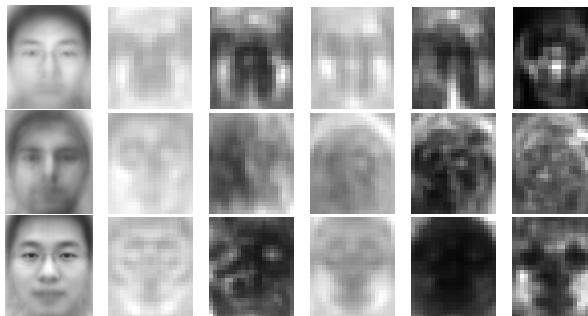


Figure 1. The first row is NUA A database [24], the second is PRINT-ATTACK database [1], and the third is CASIA database [25]. From left to right: (a) average face for each database; (b) mean and (c) variance of within-class distance (combining genuine and fake); (d) mean and variance (e) of between-class distance; (f) Fisher ratio.

ble to inaccuracy detection or tracking on face components. Moreover, users need to be highly cooperative to the system and the duration of liveness detection is relatively long. Chetty et al. [5, 6] proposed a multi-modal approach to aggrandize the difficulty of spoofing attacks. Though additional obstacles are appended to the attackers, the multi-modal methods also suffer from the operational inflexibility.

The multi-spectral methods utilize the illuminations beyond visual spectrum to tackle the anti-spoofing problem. In [20, 26], it is proved that indistinguishable faces exhibit much different properties from the genuine ones under invisible light. By selecting proper working spectrum, they can expect that inter-class difference between the genuine and fake faces are to be maximized and the final anti-spoofing decision is made properly. However, this method needs extra devices to capture face images under the invisible lights, thus it is unpractical to deploy such devices to the most of recent FR systems, which are merely based on RGB color face images.

Another kind of methods exploited the differences of appearance, including micro-textures and specular reflections between genuine and fake faces [10]. Li et al. [15] pro-

*Corresponding author.

posed a method based on the analysis of Fourier spectra. In the work of [24], Tan et al. introduced the Lambertian reflection model to discriminate the genuine and fake faces. Inspired by Tan’s work, Peixoto et al. [21] combine the DoG filters and standard Sparse Logistic Regression Model to discriminate the faces captured under bad illumination. All these methods assume that the filter response on the fake face are different from the genuine ones. However, both the assumptions of specular reflectance and blurred edges may be false in many cases. In the most recent, Maatta et al. [16] make use of the micro-textures in the holistic faces. Its anti-spoofing performance outperforms the other methods using single image on the NUAA Photograph Imposter Database [24]. The experimental results in [7] proves its efficiency in REPLAY-ATTACK database. However, dividing image into blocks rigidly, it is very sensitive to image quality changes caused by image compression or low-level devices. Moreover, It do not consider the inherent differences of discriminant abilities among different face locations.

In this paper, motivated by the works in [3, 11, 19], we introduce a component-based face liveness detection framework on the top of Fisher analysis. We segment the face image into several components, including eyes, nose, mouth, facial region in the face, as well as the informative regions surrounding canonical face region. Then, we exploit the difference among such components according to Fisher analysis in the context of liveness detection.

Contributions of this paper are bellows: (1) we exploit not only the canonical face region as described in previous face-oriented works, but also some other informative regions, such as hair, cheek, etc; (2) Compared with the methods which uniformly divide image into grids, we propose a component-based framework, which is consistent to the face structure, and thus achieve better performance; (3) Considering the difference contributions among components, we impose weights to the components by using a Fisher separation criterion [9].

2. Overview of Framework

As shown in Fig. 2, we first expand the detected face to obtain the one which we call holistic-face (H-Face). Afterward, we divide the H-Face into six components (parts), including contour region, facial region, left eye region, right eye region, mouth region, and nose region. Moreover, we further divide contour region and facial region into 2×2 grids, respectively. For all the twelve components, dense low-level features (e.g., LBP, LPQ, HOG, etc.) are extracted. Given the densely extracted local features, a component-based coding is performed based on an off-line trained codebook to obtain local codes. Then we concatenate the codes into a high-level descriptor with weights derived from Fisher criterion analysis. At last, we feed features into a support vector machine (SVM) classifier.

3. Variation after Re-Capturing

3.1. Texture Variations

We briefly analyze why local micro textures are useful for liveness detection and how they are changed during re-capturing. A significant operational difference between genuine faces and fake ones is that the former are captured by camera once, whereas the latter are obtained by re-capturing images of photos or screens. This will produce their appearance differences in three aspects: (1) Faces are blurred because of limited resolution of photos or screens and re-defocus of camera; (2) Faces appearance vary more or less for reflectance change caused by Gamma Correction of camera; (3) Face appearance also change for abnormal shading on surfaces of photos and screens.

For simplicity, we assume there is a linearity relationship between the camera output and the flux of incoming light intensity, that is, no Gamma correction for images. Based on the dichromatic reflection model [22], the image color intensity after re-capturing from a image I by a camera with Dirac delta response is formulated as:

$$I'_c(x) = [\omega_d(x)I_c(x)E_c + \omega_s(x)E_c] * G(x) \quad (1)$$

where the subscript $c \in \{r, g, b\}$, representing three color channels; E_c is the intensity of incident lights of color c ; $\omega_d(x)$ and $\omega_s(x)$ are the geometric scale factors of diffuse reflection and specular reflection, respectively. G is the gaussian blurring kernel.

For simplicity, Let denote two adjacent pixels by p_a, p_b in I . Their numerical relation is described by $\Lambda(a, b)$. We assume E is achromatic and locally consistent. Then, there are mainly three factors to affect Λ :

(1) **Diffuse reflection:** Ideally, when there is no specular reflections and gaussian blurring, $I'_c(x) = \omega_d(x)I_c(x)E_c$. In this case, if a photo is warped, then ω_d may be changed, and thus Λ as well. Therefore, shape variations can be detected by local textures;

(2) **Specular reflection:** When there is no shape variations (that is, $\omega_d(p_a) = \omega_d(p_b)$) and gaussian blurring, Λ is determined by ω_s . If there is abnormal specular reflections in images, the differences can be also easily detected by local textures;

(3) **Gaussian blurring:** When there is no shape variations and specular reflection, Λ is determined by the gaussian kernel G . The original relations Λ may be broken because of local weighted averaging.

Local textures can perceive all the possible variations during re-capturing, including gaussian blurring, diffuse and specular reflections. Because of different appearances and shapes among different regions in a real 3D face, we can infer that texture vary from one region to another in an image.

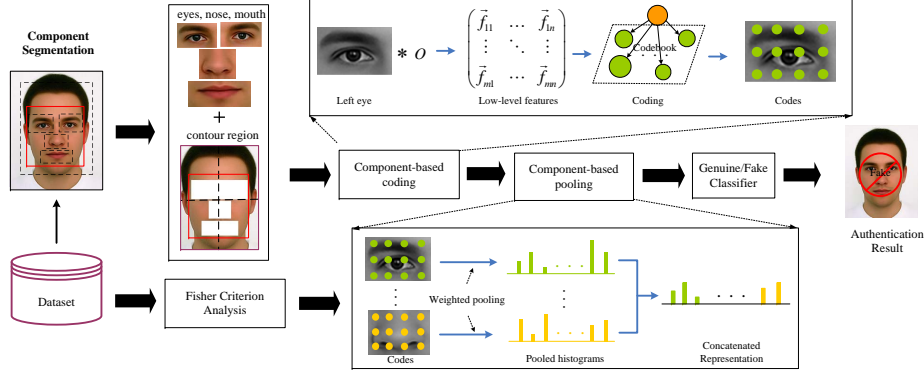


Figure 2. The flowchart of proposed framework (O represents a feature operator).

3.2. Fisher Criterion Analysis

Re-capturing changes micro textures all-around. We use Fisher ratio to describe the local difference of micro-textures between genuine faces and fake faces. To give quantitative evaluations, all H-Face images are first normalized to a consistent size $\{142, 120\}$, and then divided into 20×20 blocks with an overlap of $\{15, 15\}$. For each block, LBP features combining various scales ($LBP_{8,1}^{u2}, LBP_{8,2}^{u2}, LBP_{16,2}^{u2}$) are extracted and concatenated to be a single histogram. Then we compute the pairwise difference between blocks using Chi-Square distance:

$$d(H_i, H'_i) = \sum_{b=1}^n \frac{(H_i(b) - H'_i(b))^2}{(H_i(b) + H'_i(b))} \quad (2)$$

where H_i is the histogram of i^{th} block in a H-Face image; H'_i is the i^{th} histogram in another H-Face image; and n is the size of histogram. We first compute the differences between all the pairs of genuine faces and fake ones, denoted by $Sb = \{Sb_1, \dots, Sb_M\}$. Meanwhile, the intra differences are computed for all genuine faces and fake faces, denoted by $Swt = \{Sw_1^t, \dots, Sw_N^t\}$, $Swf = \{Sw_1^f, \dots, Sw_N^f\}$, respectively. Afterward, we compute the within class mean $m_{w,t}$, $m_{w,f}$ and variance $\sigma_{w,t}^2$, $\sigma_{w,f}^2$. The between-class mean and variance is denoted by m_b and σ_b^2 . The ratio for i^{th} block is derived by:

$$R_i = \frac{(m_{w,t} + m_{w,f} - m_b)^2}{\sigma_{w,t}^2 + \sigma_{w,f}^2 - \sigma_b^2} \quad (3)$$

Fig. 1 shows the ratio map for three databases. As we can see, NUAA and CASIA have similar ratio distributions. The PRINT-ATTACK has a different ratio distribution, which may be caused by the special fringe effects in its fake images. However, for all three databases, we can see that the higher ratios occur more densely in the contour regions, rather than inside regions which are more frequently used in previous liveness detection works.

4. Effectiveness of H-Face for Recognition

In this section, we verify the improvement of discriminative ability when exploiting contours. Besides the original face image scale, five other scales are applied to the H-Face images. The smallest size of H-Face image is $\{0.9, 0.9, 1.1, 1.3\} \times d_e$, where d_e is the pixel distance between two eyes. We amplify their values by multiply a chains of scales $\{1.0, 1.2, 1.4, 1.6, 1.8\}$. Meanwhile, different texture operators, including Local Phase Quantization (LPQ) [17], concatenated histogram of LBPs ($LBP_{8,1}^{u2}, LBP_{8,2}^{u2}, LBP_{16,2}^{u2}$) and the one with block division [16] and Histogram of Gradient (HOG) [8] are performed for the H-Face images with all scales.

As shown in Fig. 3, for NUAA database, it can be seen that there is an overall improvement on the accuracy for all the features, and the higher performance occurs at the scales of 1.6, 1.8. The results for PRINT-ATTACK database show that we can achieve a positive effect with the increase of H-Face image size when using MsLBP and LBP features, whereas a fluctuate effect when using the other features. It can be explained that the LBP operator is densely implemented for each pixel in various scales. Though the LPQ is also a densely sampled feature for each pixel, its blur-invariant property may result in a negative effect on liveness detection. For HOG feature, it is sensitive to edges in background regions. For the CASIA database, it can be seen that the increase of scales also has a positive effects on the performance for all feature types. According to the experimental results, when the scale increase to 1.6 or 1.8, accuracies of some tests start to decrease. By revisiting Fig. 1, we find that only the additional contour regions may boost the recognition performance, whereas additional background regions may have negative effects. Consequently, we choose multi-scale LBP and set a optimal scale ($=1.6$) for all the databases in the following experiments. The LBP feature for each pixel in the following experiment is extracted by concatenating four 8-bits $LBP_{8,1}, LBP_{8,2}, LBP_{8,3}, LBP_{8,4}$, and 16-bits $LBP_{16,2}$.

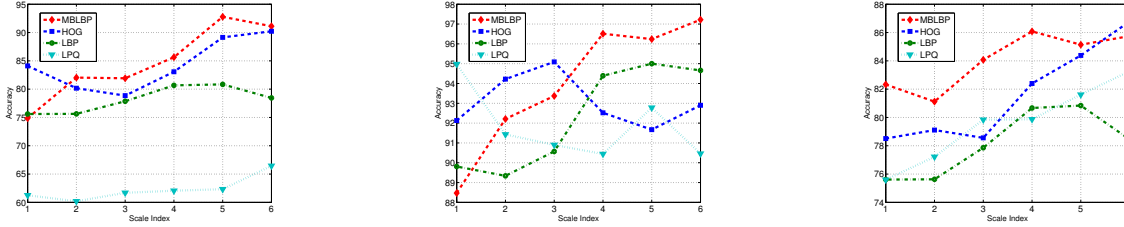


Figure 3. From left to right, the databases are: NUA, PRINT-ATTACK and CASIA databases. We choose overall test scenarios for all databases. The parameters for LPQ were $M = 5, a = 1/5, \rho = 0.9$. The cell sizes of HOG are set to be 16 and 32.

5. Component Dependent Face Coding

We propose a component dependent coding method to better make use of the differences among different regions. Compared with those method dividing image into blocks uniformly, the proposed division method is more consistent to the ratio distribution, and can retain the structure information.

5.1. Components Coding

After extract the low-level features in all the twelve components, coding is conducted to derive high-level representations of each component from low-level descriptors. In this paper, we simply choose vector quantization (VQ) [14] to code the features since it is widely used and has a simple coding algorithm, though other coding methods are also feasible. VQ algorithm is a simple yet effective coding method. The most original VQ algorithm is analogous to K-means clustering. It assign feature vector x_i a single scalar code $\alpha_i = 1_k$, which means x_i belongs to k^{th} cluster.

Mathematically, VQ coding solves a constrained least-square problem as follows:

$$\arg \min_{\mathbf{K}} \sum_{i=1}^N \|\mathbf{x}_i - \mathbf{C}_{k_i}\|^2 \quad (4)$$

where $\mathbf{K} = \{k_1, k_2, \dots, k_N\}$ denote the index of codewords for feature vectors, and $\mathbf{C} = \{\mathbf{C}_1, \mathbf{C}_2, \dots, \mathbf{C}_K\}$ is K code-word centers in the feature space.

To retain the independency among components, the coding is conducted for each component separately. The low-level feature vectors are randomly sampled in the region of component c from all the training samples, then we utilize VQ algorithm to train the codebook \mathbf{CB}_c for component c . After obtaining the codebooks, we derive codes $\mathbf{A} = \{\alpha_1, \alpha_2, \dots, \alpha_N\}$ for N pixels (patches) within a H-Face image by using the corresponding codebook, then expand each code to a vector with the same length of code-word by adding zeros to the other dimensions, denoted by $\mathbf{A} = \{\alpha_1, \alpha_2, \dots, \alpha_N\}$.

5.2. Weighted Pooling

There are two typically pooling strategies, average and max pooling. Average coding can flexibly unify the pooling results from VQ and SC algorithm to a discrete probability distribution (a normalized histogram). In this paper, we use a modified average pooling algorithm to extract the high-level image representations for each component. Our method takes the Fisher ratio maps into account. It takes the weighted average of codes over a component:

$$h_r = \frac{1}{|\Omega|} \sum_{i \in \Omega} r_i \alpha_i \quad (5)$$

where r_i is the Fisher ratio at i^{th} point. The Ratio map is first smoothed with a gaussian kernel ($w = 3, \sigma = 0.1$), and then up-sampled to one with the same size of H-Face image. After pooling, histograms for all components are concatenated into a single feature vector which is then fed into a SVM classifier.

6. Experiments

In our experiments, we use a simple cascade object detector in Matlab2012 to locate all the components in the H-Face images. All the H-Face images are resized to a consistent size $\{96, 72\}$. We randomly sample 500 feature vectors for four parts of contour region, 500 for four parts of facial region, and 300 for other components. The size of codebook is set to be 512. For classification, we use LibSVM library [4] to derive the authentication results.

We compare the recognition performance with the DoG baseline [25], and the state-of-the-art method based on MsLBP [16]. We perform the DoG baseline method and MsLBP-based method on both protocol size and the optimal size determined in this paper. For simplicity, we define some notations for tables. "DoG, Face" and "DoG, H-Face" are denoted by '1' and '2', respectively. Similarly, "MsLBP, Face" and "MsLBP, H-Face" are denoted by 3 and 4, respectively. The proposed method is denoted by '5'. Moreover, We also conduct the proposed method with holistic coding for a single image to show the efficiency of component dependent coding for each database.

6.1. Results on NUAA Database

As shown in Fig. 4, the discriminant ability of H-Face images is much better than the images of original size using both DoG features and MsLBP features. These trends are identical to those in section 4. After exploiting the component-based coding method, we further improve the recognition performance. The numerical statistics are shown in Table. 1. We can also see that the weighted pooling improves the performance much.

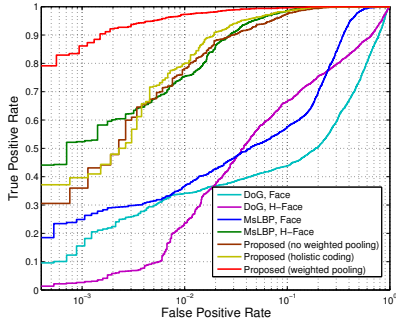


Figure 4. ROC curves of different methods for NUAA database.

Table 1. Performance comparison for NUAA database.

Metric	1	2	3	4	5
Accuracy	0.746	0.818	0.749	0.927	0.977
AUC	0.717	0.830	0.873	0.990	0.998
EER	0.359	0.233	0.239	0.048	0.019

6.2. Results on PRINT-ATTACK Database

According to the protocol of PRINT-ATTACK database, we perform three experiments with different fake subsets: i) $G+F$, "fixed" sub-database; ii) $G+F$, "hand" sub-database and iii) $G+F+H$, both of them. The experimental results are also compared with the DoG baseline method and MsLBP-based method. As shown in Table 2, the proposed method outperforms all the others in all three experiments. As we can see in Fig. 6, though there is no explicit facial structure in the Fisher ratio map, the introduction of weighted pooling still boosts the recognition ability.

Table 2. Performance on PRINT-ATTACK database.

Scenario	Metric	1	2	3	4	5
$G+F$	Accuracy	0.819	0.844	0.918	0.971	0.995
	AUC	0.978	0.990	0.980	0.988	1.000
	EER	0.068	0.055	0.068	0.026	0.003
$G+H$	Accuracy	0.852	0.884	0.898	0.958	0.991
	AUC	0.957	0.977	0.987	0.996	1.000
	EER	0.127	0.097	0.066	0.035	0.009
$G+F+H$	Accuracy	0.847	0.900	0.885	0.962	0.988
	AUC	0.967	0.983	0.991	0.994	0.999
	EER	0.096	0.073	0.049	0.038	0.012

6.3. Results on CASIA Database

In the CASIA database, we test seven scenarios according to the protocol, including *Low Quality (LQ)*, *Moderate Quality (MQ)*, *High Quality (HQ)*, *Warped Photo (WP)*, *Cut Photo (CP)*, *Video Photo (VP)* and the *Overall* test. The ROC curve of *Overall* test is shown in Fig. 5. Meanwhile, we present the corresponding accuracy, AUC and EER for all the test scenarios in Table. 3. The results indicates that the proposed method also outperforms the other methods in all the test scenarios.

Table 3. Performances on CASIA databases.

Scenario	Metric	1	2	3	4	5
<i>LQ</i>	Accuracy	0.853	0.884	0.887	0.926	0.987
	AUC	0.892	0.935	0.937	0.977	0.999
	EER	0.172	0.129	0.155	0.086	0.015
<i>MQ</i>	Accuracy	0.850	0.905	0.890	0.914	0.943
	AUC	0.829	0.926	0.941	0.972	0.987
	EER	0.245	0.153	0.120	0.085	0.050
<i>HQ</i>	Accuracy	0.774	0.854	0.863	0.907	0.931
	AUC	0.720	0.811	0.913	0.928	0.996
	EER	0.323	0.267	0.163	0.137	0.028
<i>WP</i>	Accuracy	0.732	0.810	0.786	0.859	0.930
	AUC	0.778	0.904	0.865	0.941	0.970
	EER	0.286	0.167	0.206	0.136	0.064
<i>CP</i>	Accuracy	0.780	0.845	0.821	0.882	0.953
	AUC	0.853	0.930	0.903	0.956	0.988
	EER	0.228	0.147	0.176	0.121	0.047
<i>VP</i>	Accuracy	0.686	0.800	0.861	0.952	0.997
	AUC	0.746	0.875	0.938	0.990	1.000
	EER	0.311	0.198	0.139	0.047	0.003
<i>Overall</i>	Accuracy	0.760	0.802	0.823	0.851	0.898
	AUC	0.754	0.801	0.884	0.915	0.941
	EER	0.306	0.267	0.185	0.157	0.118

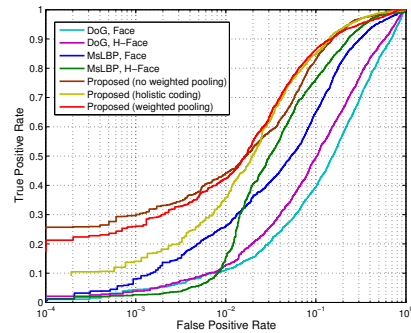


Figure 5. ROC curves for *Overall* test scenario on CASIA database.

As shown in above table, the performance on low quality samples is better than that on higher quality samples. This inspires us that the performance of liveness detection is determined by the differences between genuine faces and fake faces, instead of the quality of samples themselves. We predict that the performance can be further improved by increasing the size of codebook (In our paper, the size is set to be 512 considering the computational burden on millions of training vectors).

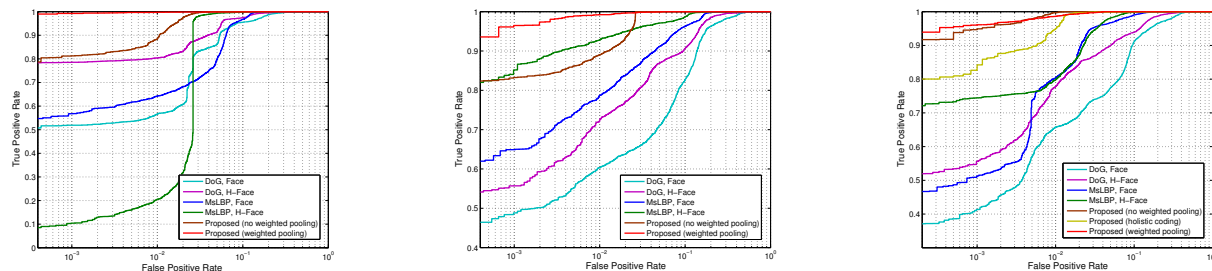


Figure 6. ROC curves for PRINT-ATTACK database. From left to right, the test scenarios are: $G+F$, $G+H$, $G+F+H$.

7. Conclusion

We have introduced a component-based coding framework for face liveness detection. We validated our recognition performance on three databases. In these databases, various spoofing types render big challenges to the previous approaches. However, by introducing H-Face, the most informative regions are retained. Meanwhile, we use Fisher criterion analysis to guide pooling procedure, which avoids interferences among regions of various discriminant abilities. As a result, the proposed method achieve better performance for all the databases.

8. Acknowledgement

This work was supported by the Chinese National Natural Science Foundation Project #61070146, #61105023, #61103156, #61105037, #61203267, National IoT R&D Project #2150510, National Science and Technology Support Program Project #2013BAK02B01, Chinese Academy of Sciences Project No. KGZD-EW-102-2, European Union FP7 Project #257289 (TABULA RASA), Guangdong-CAS Strategic Cooperation Project #2011B090300054, and AuthenMetric R&D Funds.

References

- [1] A. Anjos and S. Marcel. Counter-measures to photo attacks in face recognition: a public database and a baseline. In *International Joint Conference on Biometrics 2011*, Oct. 2011.
- [2] W. Bao, H. Li, N. Li, and W. Jiang. A liveness detection method for face recognition based on optical flow field. In *Image Analysis and Signal Processing*, pages 233–236, 2009.
- [3] K. Bonnen, B. Klare, and A. K. Jain. Component-based representation in automated face recognition. *IEEE Transactions on Information Forensics and Security*, 8(1):239–253, 2013.
- [4] C.-C. Chang and C.-J. Lin. Libsvm: A library for support vector machines. *ACM TIST*, 2(3):27, 2011.
- [5] G. Chetty. Biometric liveness checking using multimodal fuzzy fusion. In *FUZZ-IEEE*, pages 1–8, 2010.
- [6] G. Chetty and M. Wagner. Liveness detection using cross-modal correlations in face-voice person authentication. In *INTERSPEECH*, pages 2181–2184, 2005.
- [7] I. Chingovska, A. Anjos, and S. Marcel. On the effectiveness of local binary patterns in face anti-spoofing. In A. Brömme and C. Busch, editors, *BIOSIG*, pages 1–7. IEEE, 2012.
- [8] N. Dalal and B. Triggs. Histograms of oriented gradients for human detection. In *CVPR*, pages I: 886–893, 2005.
- [9] R. O. Duda and P. E. Hart. *Pattern Classification*. John Wiley and Sons, 2000.
- [10] M. M. C. *et al.* Competition on counter measures to 2-d facial spoofing attacks. In *IJCB*, pages 1–6, 2011.
- [11] H. Han, B. Klare, K. Bonnen, and A. K. Jain. Matching composite sketches to face photos: A component-based approach. *IEEE Transactions on Information Forensics and Security*, 8(1):191–204, 2013.
- [12] K. Kollreider, H. Fronthaler, and J. Bigun. Verifying liveness by multiple experts in face biometrics. In *Biometrics*, pages 1–6, 2008.
- [13] K. Kollreider, H. Fronthaler, M. I. Faraj, and J. Bigün. Real-time face detection and motion analysis with application in “liveness” assessment. *IEEE Transactions on Information Forensics and Security*, 2(3-2):548–558, 2007.
- [14] S. Lazebnik, C. Schmid, and J. Ponce. Beyond bags of features: Spatial pyramid matching for recognizing natural scene categories. In *CVPR (2)*, pages 2169–2178, 2006.
- [15] J. Li, Y. Wang, T. Tan, and A. K. Jain. Live face detection based on the analysis of fourier spectra. In *In Biometric Technology for Human Identification*, pages 296–303, 2004.
- [16] J. Maatta, A. Hadid, and M. Pietikainen. Face spoofing detection from single images using micro-texture analysis. In *Biometrics (IJCB), 2011 International Joint Conference on*, pages 1–7, oct. 2011.
- [17] V. Ojansivu and J. Heikkilä. Blur insensitive texture classification using local phase quantization. In *Image and Signal Processing*, pages 236–243, 2008.
- [18] G. Pan, L. Sun, Z. Wu, and S. Lao. Eyeblink-based anti-spoofing in face recognition from a generic webcam. In *ICCV*, pages 1–8, 2007.
- [19] K. Pan, S. C. Liao, Z. J. Zhang, S. Z. Li, and P. R. Zhang. Part-based face recognition using near infrared images. In *OTCBVS Benchmark Dataset Collection*, pages 1–6, 2007.
- [20] I. Pavlidis and P. Symosek. The imaging issue in an automatic face/disguise detection system. In *Computer Vision Beyond the Visible Spectrum: Methods and Applications*, page 15, 2000.
- [21] B. Peixoto, C. Michelassi, and A. Rocha. Face liveness detection under bad illumination conditions. In *ICIP*, pages 3557–3560, 2011.
- [22] S. Shafer. Using color to separate reflection components. *Color Research and Applications*, 10:210–218, 1985.
- [23] L. Sun, G. Pan, Z. Wu, and S. Lao. Blinking-based live face detection using conditional random fields. In *ICB*, pages 252–260, 2007.
- [24] X. Tan, Y. Li, J. Liu, and L. Jiang. Face liveness detection from a single image with sparse low rank bilinear discriminative model. In *ECCV (6)*, pages 504–517, 2010.
- [25] Z. Zhang, J. Yan, S. Liu, Z. Lei, D. Yi, and S. Z. Li. A face anti-spoofing database with diverse attacks. In A. K. Jain, A. Ross, S. Prabhakar, and J. Kim, editors, *ICB*, pages 26–31. IEEE, 2012.
- [26] Z. Zhang, D. Yi, Z. Lei, and S. Z. Li. Face liveness detection by learning multispectral reflectance distributions. In *FG*, pages 436–441, 2011.